Using Particle Swarm Optimization for Power System Stabilizer and energy storage in the SMIB system under load shedding conditions

Mansur Mansur[1*], Muhammad Ruswandi Djalal[2]
[1]Department of Electrical Engineering, Halu Oleo University, Indonesia
[2]Department of Mechanical Engineering, State Polytechnic of Ujung Pandang, Indonesia

Abstract
Generator instability, which manifests as oscillations in frequency and rotor angle, is brought on by sudden disruptions in the power supply. Power System Stabilizer (PSS) and Energy Storage are additional controllers that enhance generator stability. Energy storage types include superconducting magnetic (SMES) and capacitive (CES) storage. If the correct settings are employed, PSS, SMES, and CES coordination can boost system performance. It is necessary to use accurate and effective PSS, SMES, and CES tuning techniques. Artificial intelligence techniques can replace traditional trial-and-error tuning techniques and assist in adjusting controller parameters. According to this study, the PSS, SMES, and CES parameters can be optimized using a method based on particle swarm optimization (PSO). Based on the investigation's findings, PSO executes quick and accurate calculations in the fifth iteration with a fitness function value of 0.007813. The PSO aims to reduce the integral time absolute error (ITAE). With the addition of a load-shedding instance, the case study utilized the Single Machine Infinite Bus (SMIB) technology. The frequency response and rotor angle of the SMIB system are shown via time domain simulation. The analysis's findings demonstrate that the controller combination can offer stability, reducing overshoot oscillations and enabling quick settling times.

INTRODUCTION

Due to the governor response being extremely sluggish in comparison to the excitation system response, the dynamic stability research makes the assumption that the torque change caused by the governor response is minimal. The excitation system is therefore the governing factor. Particularly for low-frequency oscillations, adding an amplifier excitation circuit is less effective at stabilizing the system [1, 2, 3]. Change at low frequencies between 0.2 and 2.0 Hz .

Lower frequencies have the potential to cause oscillations between regions, necessitating further controls such as Power System Stabilizer (PSS) management. The PSS, a control mechanism that is added to the generator excitation, further dampens the generator excitation [4]. Additionally, it reduces regional or global oscillations on the generator due to variations in predetermined variable values [5]. Large amounts of power can be simultaneously stored and released using superconducting magnetic energy storage (SMES). While a device for storing and discharging power, Capacitive Energy Storage (CES) stores energy in the form of an electric field in a capacitor [6][7]. Combining energy storage based on SMES and CES can enhance system performance if the correct parameters are employed. Correct and ideal PSS, SMES, and CES settings are required to stabilize the system and decrease oscillations to achieve the best outcomes [8]. The optimization of

intelligent techniques, or what is usually referred to as artificial intelligence, can be used to tune these parameters.

The Swarm Intelligence group, one form of paradigm development used to address optimization issues, includes Particle Swarm Optimization (PSO). The behaviour of particles in groups searching for food sources serves as motivation for problem-solving [9][10]. This study also employs the PSO approach to enhance control parameters like [11, 12, 13]. The use of intelligent methods to optimize generator control parameters has been covered in several studies, and the outcomes provided to the system are outstanding in preserving generator stability. Examples of these methods include firefly method [14], bat algorithm [15, 16, 17], flower pollination [18], imperialist competitive [19], and cuckoo search [20][21].

The controller's optimal parameter tuning will significantly impact the system's ability to stabilize [22]. An optimization method utilizing PSO is used to quickly get parameter values because the range of equipment parameters is broad and diverse. The objective function minimizes the Integral Time Absolute Error (ITAE), and the response value is determined by examining the overshoot and settling time values [23]. Overshoot is the occurrence when a signal or function exceeds its target, while settling time is the time required to reach the target The case study system is Single Machine Infinite Bus (SMIB). An infinite number of buses are connected to one or more generators as part of the SMIB electric power subsystem [24][25]. Then compare the simulation outcomes of the system without control, SMIB-PSS, SMIB-SMES, CES, SMES-CES, and with the suggested technique PSS-SMES-CES with PSO to examine the simulation outcomes. The authors of this study used an intelligent PSO-based method to solve the optimization problem of choosing the PSS-SMES-CES parameters on the SMIB system.

SYSTEM MODELING
Synchronous Machine Linear Modeling

An infinite bus connected to a generator represents the Single Machine Infinite Bus (SMIB) system. SMIB made the following assumptions in this paper: the system was supposed to be in balance, the load was assumed to be static; and the saturation of the core generator and resistance resistor was minimal [26]. In Figure 1, the SMIB linear model is displayed.
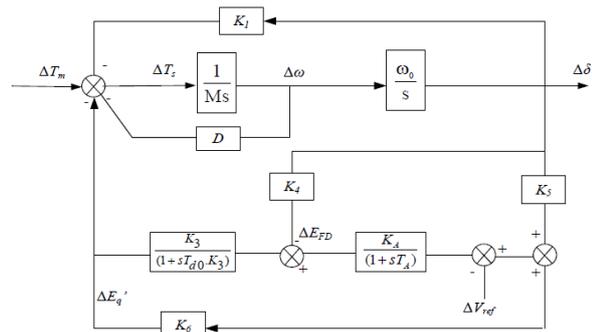

Figure 1. Linear Modeling of Synchronous Machines

Excitation Modeling

The excitation system controls the generator's voltage, current, and power factor. If there is a change in the output of the generator, then the excitation system regulates the generator to adjust and establish a new equilibrium point. One component of the method where this exciter can control generator output characteristics like the voltage, current, and power factor is the excitation equipment [27]. The excitation model alludes to the modelling performed by IEEE, which is depicted in Figure 2 [28].

K_A is the amplifier gain constant, K_F is the filtered gain constant, K_E is the exciter gain constant, T_A is the amplifier response time, T_E is the exciter response time, T_F is the filtered response time, and ΔU_2 is the engine control signal change.

Governor Modeling

To maintain a constant rotor speed for the generation system, the governor, a component of the generator unit, controls the fuel supply (steam or water). A feedback function will take place if the load on the generator changes, which the governor controls to vary the rotation of the rotor. The governor is a controller that modifies the mechanical torque Tm, the generator's input, by changing its value [28]. In Figure 3, governor modelling is displayed.
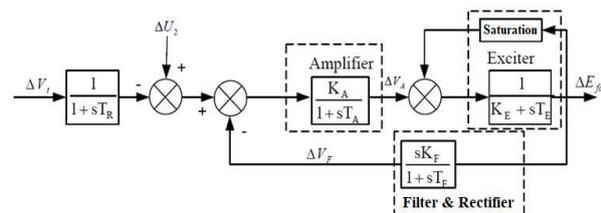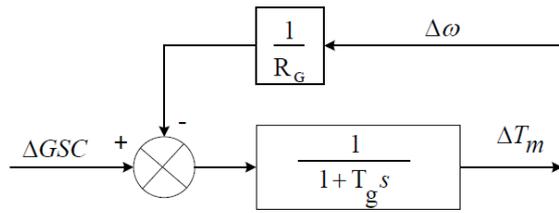

Figure 2. Excitation Block Diagram

Figure 3. Governor Modeling

K_g is Gain constant = $1/R_G$, T_g is the Governor time constant, R_G is the Governor groop constant, and ΔGSC is Governor Speed Changer.

Turbine Modeling

The steam power turbine model from the IEEE model is utilized for the turbine [29]. Figure 4 depicts a turbine model.

ΔY is valve height change, T_{wi} is steam turbine response time, T_{ga} is steam turbine governor response time, K_{ga} is steam turbine governor gain, R is steam turbine governor constant, and ΔU_1 is feedback control signal change.

Modeling Single Machine Infinite Bus (SMIB)

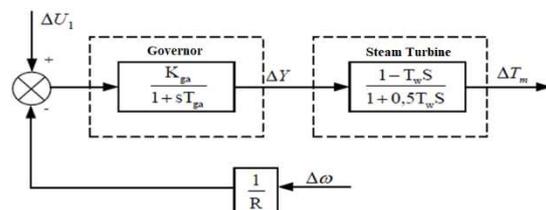Figure 5 displays the overall modeling of the Single Machine Infinite Bus system [30].
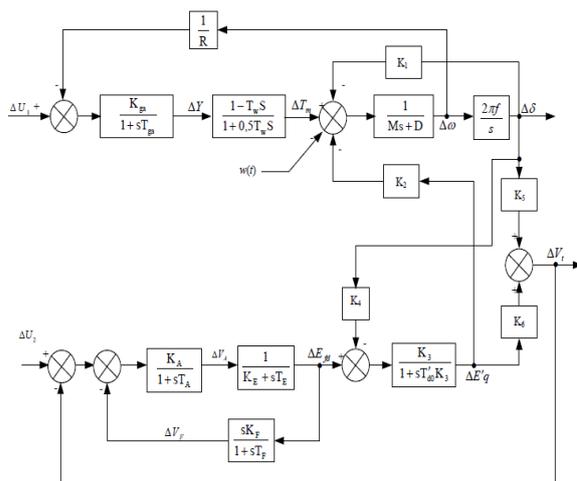

Figure 4. Turbine Modeling

Figure 5. SMIB Modeling

Power System Stabilizer Modeling

A tool called the Power System Stabilizer can be used to make the power system more stable. Figure 6 depicts the PSS modelling used in this investigation.

Block Gains are used to modifying the reinforcement amount to produce the required torque. A PSS steady-state output bias from the Washout block will change the generator terminal voltage. The PSS is anticipated to only react to brief changes in the generator rotor speed signal, not DC offset signals. To account for the phase lag between the excitation input and the generator torque, the Lead-Lag block performs as a generator with proper phase-lead characteristics. The PSS action on the AVR is as anticipated because the PSS output is constrained. The AVR, for instance, lowers the generator's terminal voltage when there is an unload. The PSS produces a control signal to raise the voltage concurrently (because the speed of the generator rotor increases when the load is released).

Superconducting Magnetic Energy Storage Modeling

SMES is a tool for concurrently storing and releasing enormous amounts of power. SMES uses superconducting coils that a cryogenic system cools to create a magnetic field that holds energy. a SMES with superconducting coils, a cryogenic cooling system, and a power conditioning system (PCS) with control and protective features coupled to the electrical power system. The power electronics connector of the SMES coil is also called PCS. The SMES schematic diagram is displayed in Figure 7.
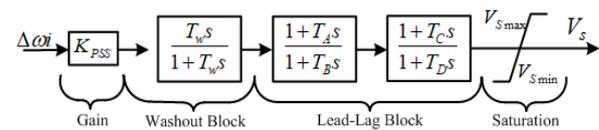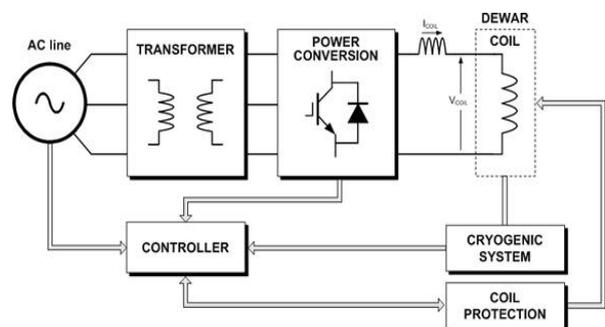

Figure 6. PSS Modeling

Figure 7. SMES schematic diagram

$$V_{SM} = D * V_{DC} \tag{1}$$

$$-V_{SM} = (1-D) * V_{DC} \tag{2}$$

$$I_{SM} = \frac{1}{L_{SM}} \int_{t_0}^{t} V_{DC} d\tau + I_{SM0} \tag{3}$$

$$P_{SM} = V_{SM} I_{SM} \tag{4}$$

$$W_{SM} = \frac{1}{2} L_{SM} I_{SM}^2 \tag{5}$$

Equation (1), where V_{DC} is the voltage in the capacitor DC link, D is the duty cycle, and VSM is the voltage in the SMES coil, represents the SMES charging mode. SMES is current is represented by (3), while SMES discharging mode is represented by (2). The energy delivered and stored by SMES is represented by(4), while energy stored in the SMES coil is represented by (5). The SMES arrangement is depicted in Figure 8.

To balance the power control on the generator, SMES is installed at the generator terminals. From several SMES reference equations, the SMES-PID block diagram can be constructed, as shown in Figure 9.

Capacitive Energy Storage Modeling
CES is a power storage and distribution system. CES uses an electric field to store energy in a capacitor. A CES comprises a Power Conversion System (PCS) and a storage capacitor. The CES schematic is shown in Figure 10.
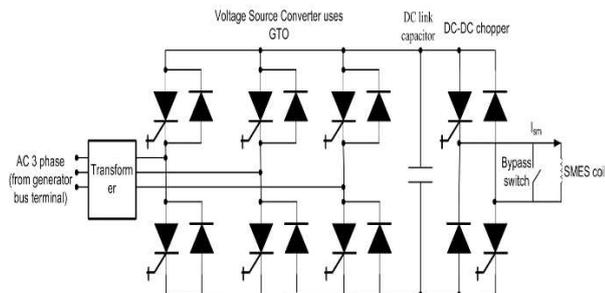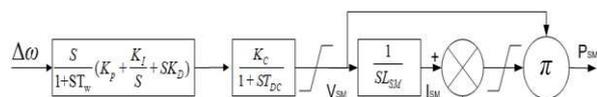

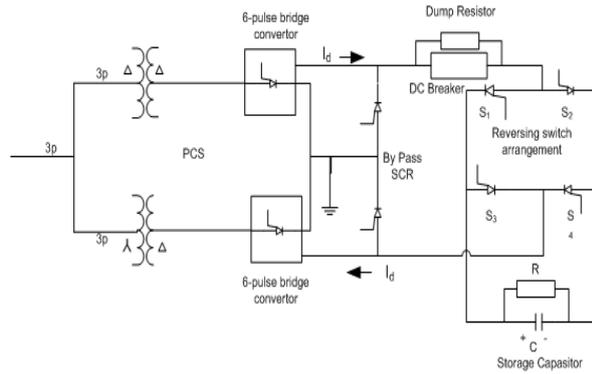Figure 8. SMES Configuration

Figure 9. SMES-PID Modeling

Figure 10. CES

A capacitance C is created by connecting several capacitors in parallel. CES uses a resistor R linked in parallel to the capacitor to mimic leaking losses and dielectric capacitor banks. A 12-pulse PCS connects the storage capacitor to the grid. A DC rectifier plus a DC to AC inverter make up PCS. In this case, the bypass thyristor offers a conduit for the current Id in case of a converter failure. If the converter fails, the DC Breaker sends the current I_d to a location that can drain the energy resistor R_D. As in the equation, the bridge voltage E_d considers losses (7).

$$E_d = 2E_{d0} \cos\alpha - 2I_d R_D \tag{6}$$

$$E_{d0} = \frac{[E_{d\max}^2 + E_{d\min}^2]^{1/2}}{2} \tag{7}$$

Imagine that the capacitor voltage is too low and that another fault arises before it reaches its average value. In that situation, a failure will demand more energy from the capacitor, which can result in intermittent control. To solve this issue, the lower limit of the capacitor voltage is set at 30% of the rating value E_{d0}.

$$E_{d\min} = 30E_{d0} \tag{8}$$

To get ready for the next load disturbance, the CES unit must quickly return to its initial value after the load disturbance. As shown in Figure 11, the CES control loop uses the capacitor voltage deviation as a negative feedback signal to ensure speedy voltage recovery.
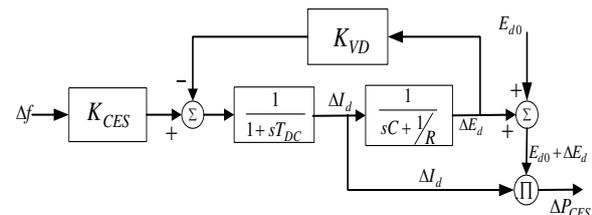

Figure 11. CES Block Diagram

METHOD
Particle Swarm Optimization
PSO stands for population-based optimization. Several particle populations initially span a problem space in PSO. Swarms are the name given to these scattered particles. The presence of this particle and any potential value it might have been recorded in this particle. The exchange of information between particles will allow us to determine which ones are in the position that will produce the best movement-related outcomes. Based on this knowledge, other particles will go there using a velocity motion function. Each particle chooses its position during flight based on its own experience (P_{best}) and the experience of other particles (G_{best}). In Figure 12, the procedure for locating P_{best} and G_{best} is depicted.

Each particle's speed can be calculated from (9).

$$v_{k+1} = w.v_k + c_1 rand \times (P_{best} - x^k) + c_2 rand \times (G_{best} - x^k) \quad (9)$$

Based on particle velocity, P_{best} and G_{best} can be computed using (9). You can get the most current position from (10).

$$x^{k+1} = x^k + v_{k+1} \quad . \quad k = 1,2 \dots n \quad (10)$$

For the following terms, X^k stands for the search point base, X^{k+1} for the search position, V^k for speed, V^{k+1} for modified speed, V_{pbest} for speed based on P_{Best}, V_{gbest} for speed based on G_{best}, n for number of particles in group, m for number of members in particle, p_{best-i} for P_{best} from k, G_{best-i} for G_{best} from group, w for weight, and c_i for weight coefficient. The positive constants are c_1 and c_2, and the random numbers are r_1 and r_2.

The following is the iteration function of k and w is the weight of inertia (11).

$$w(k) = w_{max} - \left(\frac{w_{max} - w_{min}}{max.iter}\right) \times k \quad (11)$$

In order to ensure that all dimensions move at the same pace, the maximum speed is as follows (12).

$$v^{max} = \frac{(x^{max} - x^{min})}{N} \quad (12)$$

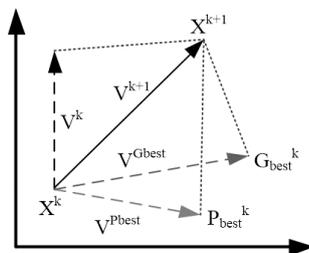N stands for the maximum iterations.

Figure 12. Searching PSO conceph [31]

Table 1 lists the PSO parameters used in this investigation. To test the accuracy of PSO in optimization, the Ant Colony Optimization (ACO) method is used as a comparison. The ACO parameters are shown in Table 1.

PSO Implementation for Computing
The Integral Time Absolute Error (ITAE) is an objective function used to evaluate a system's stability.

$$ITAE = \int_0^t t|\Delta\omega(t)|dt \quad (13)$$

The PSS-SMES-CES parameters tuned by Particle Swarm Optimization are T_{dc}, K_{smes}, K_{pss}, T_1, T_2, T_3, T_4, and K_{DE}.

The outstanding value will considerably impact the SMIB developed for this study's response performance. To determine the ideal value, the PSO algorithm needs to be calculated. The optimization convergence graph using the PSO technique is shown in Figure 13. The fitness function value of convergence describes an optimization problem's best criteria. The convergence graph for PSS-SMES-CES value optimization using PSO is shown in Figure 13, and it can be observed from the chart that the PSO method completes the optimization process quickly. The algorithm's fifth iteration, which discovered the excellent value with a fitness value of 0.007813, demonstrates this.

Table 1. Parameters for PSO

PSO		ACO [6]	
Parameters	Value	Parameters	Value
Particles	30	Number of Ants	6
Most Iterations	50	Max Iteration	50
The quantity of variables	8	Pheromone	0.9
C2 Social Constant	2	Beta	2
C1 Cognitive Constant	2		
W Moment Inertia	0.9		
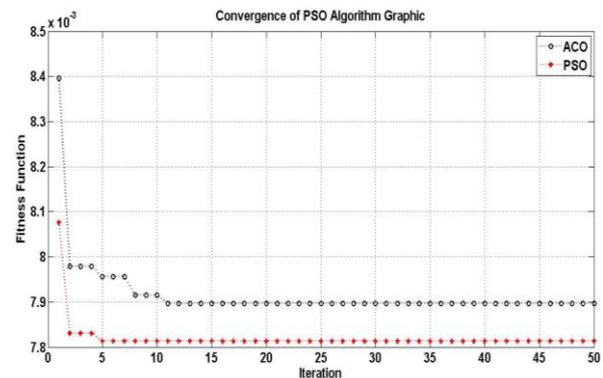
Figure 13. Convergence Graph

Table 2. PSO Optimization Limits and Results

Parameter	Limits		Results
	Lower	Upper	
T_{dc}	0	11	0.0288
K_{smes}	0	200	199.5044
K_{pss}	0	70	64.3794
T_1	0	1	0.0397
T_2	0	1	0.0401
T_3	0	1	1.1169
T_4	0	1	5.4299
T_{dc1}	0	1	0.0523
K_{DE}	0	100	94.9493

While using the ACO method, the optimization process converges at the 11th iteration, reaching a fitness function value of 0.007897. These results indicate that PSO outperforms ACO in terms of performance.

Based on the objective function used, in the 5th iteration, PSO obtains the optimal values of the parameters T_{dc}, K_{smes}, K_{pss}, T_1, T_2, T_3, T_4, T_{dc1}, and K_{DE}. Table 2 lists the restrictions and outcomes of the PSS-SMES-CES parameters PSO tuned for optimization.

RESULTS AND DISCUSSION

Employing time domain simulation to examine the system frequency response and SMIB rotor angle. Load shedding variations are applied to the SMIB system to verify the system's stability. Load shedding has an impact on the generator due to sudden load shedding.

SMIB Frequency Response

Reviewing the SMIB system's frequency stability response is the first step of the investigation. Figure 14 displays the simulation findings. Figure 14 shows the frequency response simulation results for SMIB using various control strategies. According to the simulation results, a change in the load of 0.01 pu in the first second disturbs the SMIB system. Then, there is a load shedding during the 20th second of 0.005 pu. When a load is added during the first load shift, the electrical and mechanical torques are not balanced because the electrical power (P_e) and mechanical power (P_m) are not equal in this scenario. This circumstance likewise alters the electric frequency (Δf). The rotor rotation speed $(\Delta \omega)$ deviates from equilibrium during this instability. The frequency response graph in this situation declines before stabilizing. The control system's operation must then resume operating in steady-state conditions. Table 3 displays the features of the overshoot reaction in this circumstance.

The system's overshoot characteristics are shown in Table 3 when a load change, like an increased load, happens in the first second.

Table 3. Deviation in SMIB Frequency

Deviation	Overshoot (pu)
Uncontrol	-0.0002403 & 0.0001873
PSS-PSO	-0.0001992 & 8.215e-05
SMES-PSO	-0.0001512 & 5.479e-06
CES-PSO	-0.0001394 & 1.057e-07
SMES-CES-PSO	-0.0001078 & 9.557e-07
SMES-CES-PSS-PSO	-0.0001033 & 3.283e-07

The unmanaged SMIB system had an overshoot of -0.0002403 & 0.0001873 pu with a settling period of 15.2 seconds. The SMIB system controlled by PSS had an overrun of -0.0001992 & 8.215e-05 pu with a settling time of 5.6s. The SMIB system managed by SMES recorded an overshoot of -0.0001512 & 5.479e-06 pu with a settling time of 3.6s. The SMIB system operated by CES had an overshoot of -0.0001394 & 1.057e-07 pu with a settling time of 3.2s. SMIB, managed by SMES-CES, had an overshoot of -0.0001078 & 9.557e-07 pu and a settling time of 3.2s. With the suggested method using PSS-SMES-CES, the smallest overshoot is -0.0001033 & 3.283e-07.

The electrical power (P_e) then changes due to the following load change, which takes the form of a drop in load. The mechanical and electrical torque are not balanced in this situation because the electrical power is not equal to the mechanical power (P_m) $P_e < P_m$. This circumstance likewise alters the electric frequency (Δf). The rotor rotation speed $(\Delta \omega)$ deviates from equilibrium during this instability. The frequency response graph in this situation increases before stabilizing. The control system's operation must then resume operating in steady-state conditions. Table 4 displays the parameters of the overshoot response under these circumstances. The system's electrical frequency response (Δf) is depicted in Figure 14.

The characteristics of the system overshoot, when there is a load change at the 20th second are shown in Table 4. The SMIB system's uncontrolled overshoot was -9.048e-05 & 0.0001202 pu with a 34-second settling time. A settling time of 25s and an overshoot of -4.088e-05 & 9.764e-05 pu were recorded by the SMIB system under PSS control.

Table 4. Deviation in SMIB Frequency

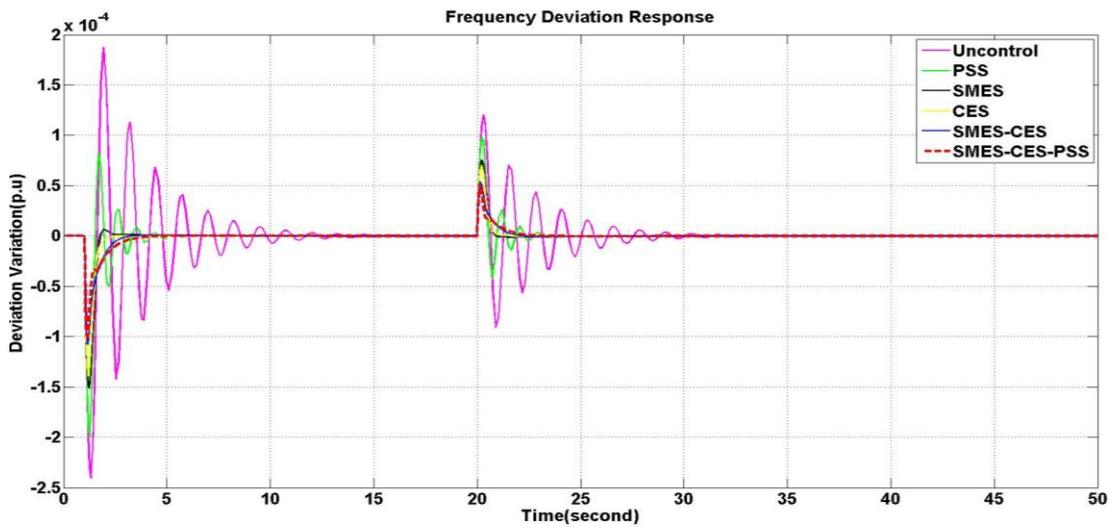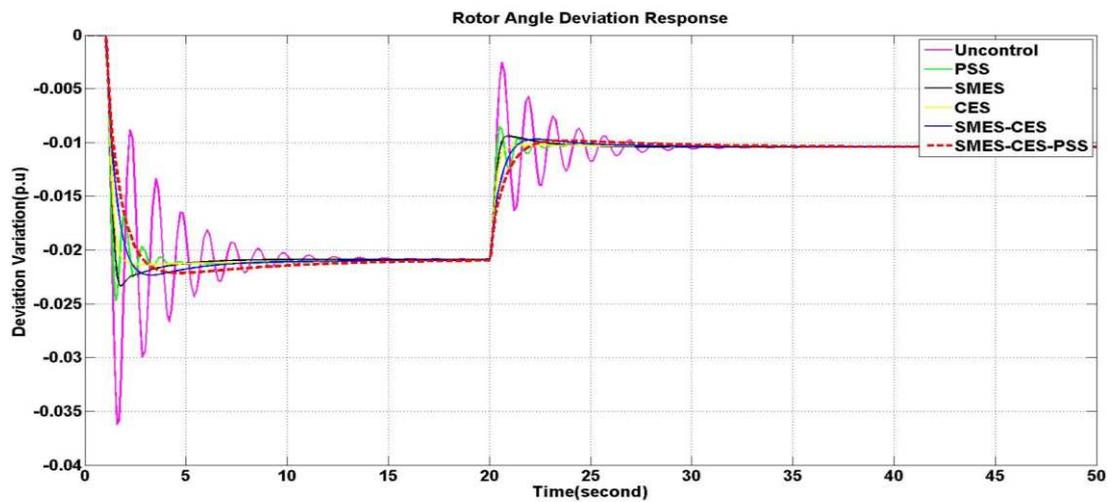| Deviation	Overshoot (pu)
Uncontrol	-9.048e-05 & 0.0001202
PSS-PSO	-4.088e-05 & 9.764e-05
SMES-PSO	-1.145e-06 & 7.547e-05
CES-PSO	0 & 7.547e-05
SMES-CES-PSO	0 & 5.409e-05
SMES-CES-PSS-PSO	0 & 5.188e-05

Figure 14. SMIB Frequency Response

Figure 15. SMIB Rotor Angle Response

A settling time of 24.74s and an overshoot of -1.145e-06 & 7.547e-05 pu were recorded by the SMIB system under SMES control. A settling time of 24.14s and an overshoot of 0 & 7.547e-05 pu were obtained by the SMIB system under CES control. A settling time of 22.43s and an overshoot of 0 & 5.409e-05 pu were brought by SMIB under SMES-CES control. The smallest overshoot is 0 & 5.188e-05 pu with the suggested method using PSS-SMES-CES.

SMIB Rotor Angle Response

The ensuing investigation examines the SMIB rotor's angle response as it operates with PSS-PID control installed. A change of 0.05 pu in 1s was used in this study's SMIB test. A rise and increase in load are the intended changes. Electrical power will also alter due to the increased load and rise. The rotor can accelerate if the

generator's mechanical power is more significant than its electrical power. Compared to the conditions before the disturbance, as shown in Figure 15, this rotor acceleration will have a negative or decreasing effect on the rotor angle response. The values of overshoot and settling time are the observed reaction to the change in rotor angle, as indicated in Table 5.

Table 5. Deviation of SMIB Rotor Angle

Deviation	Overshoot (pu)
Uncontrol	-0.03623
PSS-PSO	-0.02471
SMES-PSO	-0.02308
CES-PSO	-0.02134
SMES-CES-PSO	-0.02233
SMES-CES-PSS-PSO	-0.02212

When there is a change in load in the first second in the form of an additional load, Table 5 displays the overshoot characteristics of the system rotor angle. The SMIB system's uncontrolled overshoot was -0.03623 pu with an 18.5s settling period. A settling time of 6.4s and an overshoot of -0.02471 pu were attained by the SMIB system under PSS control. The SMIB system under SMES management recorded a -0.02308 pu overshoot with a 9.2s settling time. The SMIB system under CES control recorded an overshoot of -0.02134 pu and an 8-second settling time. SMIB under SMES-CES management had an overrun of -0.02233 pu and a 4.3s settling time. The least overshoot is then achieved using the suggested strategy employing PSS-SMES-CES.

Then, at the 20th second, there is the following load change: a decrease in load. In this situation, the generator's mechanical power is lower than its electrical power, which causes the rotor to slow down. The rotor's slowdown will also impact the change in angle, causing the angle response to be more favorable than before the disturbance. This occurs due to the magnetic connection pushing the stator field toward the rotor field, increasing the generator's rotor angle, as seen in Figure 15. Table 6 displays the system's overshoot characteristics under these circumstances.

Table 6 displays the system rotor angle's overshoot characteristics when the load changes at the 20th second. With a 30-second settling time, the unmanaged SMIB system recorded an overrun of -0.0159 pu. With a settling time of 25.17s, the SMIB system under PSS management had an overrun of -0.01235pu. With a settling time of 24s, the SMIB system under SMES management recorded an overrun of -0.009407 pu. With a settling time of 25s, the SMIB system under CES control recorded an overshoot of -0.01024 pu. With a settling time of 24.5s, SMIB under SMES-CES management recorded an overrun of -0.009698 pu. The minor overshoot with the suggested method employing PSS-SMES-CES is -0.009833 pu with a settling time.

Table 6. Deviation of SMIB Rotor Angle

Deviation	Overshoot (pu)
Uncontrol	-0.0159
PSS-PSO	-0.01235
SMES-PSO	-0.009407
CES-PSO	-0.01024
SMES-CES-PSO	-0.009698
SMES-CES-PSS-PSO	-0.009833

The results of this study indicate that there is an increase in SMIB performance when load shedding occurs, utilizing the proposed control scheme based on PSS and Energy Storage. Compared to the previous research conducted [25], the proposed control scheme is based on conventional PSS and PID. This study also demonstrates that the PSO-based tuning method yields a lower fitness function compared to the comparison method used in previous studies based on ACO.

CONCLUSION

This research proposes a PSS-based SMIB control design and energy storage under load shedding conditions. Study of system reliability in this condition is important to do for generator performance. To optimize the performance of PSS-Energy Storage, the PSO method is used for optimal parameter optimization. The PSO algorithm performs optimization well, showing that the optimization time is fast. The PSO computation converges in the 5th iteration, and the optimal parameter tuning is obtained with a fitness function value of 0.007813.

Comparing an uncontrolled system to optimal tuning, the SMIB frequency response is excellent. Improved system responsiveness, where the controller can offer stability to reduce overshoot oscillations, and quick settling time performance for the system to reach a steady state condition are indicators. Lowering the overshoot in this system requires properly tweaking the SMES-CES-PSS parameters.

REFERENCES

[1] A. Bagheri, M. T. Salam, J. L. P. Velazquez, and R. Genov, "Low-Frequency Noise and Offset Rejection in DC-Coupled Neural Amplifiers: A Review and Digitally-Assisted Design Tutorial," *IEEE Transactions on Biomedical Circuits and Systems,* vol. 11, no. 1, pp. 161-176, 2017, doi: 10.1109/TBCAS.2016.2539518.

[2] M. Saadatmand, G. B. Gharehpetian, A. Moghassemi, J. Guerrero, P. Siano, and H. Haes Alhelou, "Damping of Low-Frequency Oscillations in Power Systems by Large-Scale PV Farms: A Comprehensive Review of Control Methods," *IEEE Access,* vol. 9, pp. 72183-72206, 2021, doi: 10.1109/ACCESS.2021.3078570.

[3] P. S. Kundur and O. P. Malik, *Power system stability and control,* McGraw-Hill Education, 2022.

[4] R. D. Muhammad, Y. Y. Muhammad, S. Herlambang, and U. K. Awan, "Small-Signal-Stability Enhancement using a Power-System Stabilizer based on the Cuckoo-Search Algorithm against Contingency N-1 in the Sulselrabar 150-kV System," *Makara*

Journal of Technology, vol. 22, no. 1, pp. 1-8, 2018, doi: 10.7454/mst.v22i1.3497.

[5] M. R. Djalal, I. Robandi, and M. A. Prakasa, "Stability Enhancement of Sulselrabar Electricity System Using Mayfly Algorithm Based on Static Var Compensator and Multi-Band Power System Stabilizer PSS2B," *IEEE Access,* vol. 11, pp. 57319-57340, 2023, doi: 10.1109/ACCESS.2023.3283598.

[6] A. M. S. Yunus, A. Abu-Siada, M. R. Djalal, and J. X. Jin, "Optimal Design of SMES and PSS for Power System Stability based on Ant Colony Optimization," in *2020 IEEE International Conference on Applied Superconductivity and Electromagnetic Devices (ASEMD)*, 16-18 Oct. 2020 2020, pp. 1-2, doi: 10.1109/ASEMD49065.2020.9276201.

[7] I. T. Yuniahastuti, I. Anshori, and I. Robandi, "Load frequency control (LFC) of micro-hydro power plant with Capacitive Energy Storage (CES) using Bat Algorithm (BA)," in *2016 International Seminar on Application for Technology of Information and Communication (ISemantic)*, 5-6 Aug. 2016 2016, pp. 147-151, doi: 10.1109/ISEMANTIC.2016.7873828.

[8] H. Setiadi and K. O. Jones, "Power system design using firefly algorithm for dynamic stability enhancement," *Indonesian Journal of Electrical Engineering and Computer Science,* vol. 1, no. 3, pp. 446-455, 2016, doi: 10.11591/ijeecs.v1.i3.pp446-455.

[9] B. Crawford, R. Soto, F. Johnson Parejas, E. Monfroy, and F. Paredes, "A Max–Min Ant System algorithm to solve the Software Project Scheduling Problem," *Expert Systems with Applications,* vol. 41, pp. 6634–6645, 11/01 2014, doi: 10.1016/j.eswa.2014.05.003.

[10] M. Braik, A. Sheta, and H. Al-Hiary, "A novel meta-heuristic search algorithm for solving optimization problems: capuchin search algorithm," *Neural Computing and Applications,* vol. 33, no. 7, pp. 2515-2547, 2021/04/01 2021, doi: 10.1007/s00521-020-05145-6.

[11] S. M. H. Mousakazemi and N. Ayoobian, "Robust tuned PID controller with PSO based on two-point kinetic model and adaptive disturbance rejection for a PWR-type reactor," *Progress in Nuclear Energy,* vol. 111, pp. 183-194, 2019, doi: 10.1016/j.pnucene.2018.11.003.

[12] H. Housny, E. A. Chater, and H. el Fadil, *Fuzzy PID Control Tuning Design Using Particle Swarm Optimization Algorithm for a Quadrotor,* 2019, pp. 1-6.

[13] Y. Liu *et al.*, "Self-Tuning Control of Manipulator Positioning Based on Fuzzy PID and PSO Algorithm," (in English), *Frontiers in Bioengineering and Biotechnology,* Original Research vol. 9, 2022, doi: 10.3389/fbioe.2021.817723.

[14] M. Singh, R. N. Patel, and D. D. Neema, "Robust tuning of excitation controller for stability enhancement using multi-objective metaheuristic Firefly algorithm," *Swarm and Evolutionary Computation,* vol. 44, pp. 136-147, 2019, doi: 10.1016/j.swevo.2018.01.010.

[15] A. Alharbi, W. Alosaimi, H. Alyami, H. T. Rauf, and R. Damaševičius, "Botnet Attack Detection Using Local Global Best Bat Algorithm for Industrial Internet of Things," *Electronics,* vol. 10, no. 11, p. 1341, 2021, doi: 10.1016/j.eswa.2019.112945.

[16] H. Tang, W. Sun, H. Yu, A. Lin, and M. Xue, "A multirobot target searching method based on bat algorithm in unknown environments," *Expert Systems with Applications,* vol. 141, p. 112945, 2020, doi: 10.1016/j.eswa.2019.112945.

[17] N. Talbi, "Design of Fuzzy Controller rule base using Bat Algorithm," *Energy Procedia,* vol. 162, pp. 241-250, 2019, doi: 10.1016/j.egypro.2019.04.026.

[18] S. Nadweh, O. Khaddam, G. Hayek, B. Atieh, and H. Haes Alhelou, "Optimization of P& PI controller parameters for variable speed drive systems using a flower pollination algorithm," *Heliyon,* vol. 6, no. 8, p. e04648, 2020, doi: 10.1016/j.heliyon.2020.e04648.

[19] M. Elsisi, "Design of neural network predictive controller based on imperialist competitive algorithm for automatic voltage regulator," *Neural Computing and Applications,* vol. 31, no. 9, pp. 5017-5027, 2019, doi: 10.1007/s00521-018-03995-9.

[20] M. R. Djalal and I. Robandi, "Improving The Stability of Sulselrabar System with Dual Input Power System Stabilizer Based on Imperialist Competitive Algorithm," in *2022 International Conference on Electrical Engineering, Computer and Information Technology (ICEECIT)*, 22-23 Nov. 2022 2022, pp. 262-268, doi: 10.1109/ICEECIT55908.2022.10030389.

[21] M. Saini, M. R. Djalal, and A. M. S. Yunus, "Optimal Coordination PID-PSS Control Based on Craziness Particle Swarm Optimization In Sulselrabar System," in *2022 5th International Seminar on Research of Information Technology and Intelligent Systems (ISRITI)*, 8-9 Dec. 2022 2022, pp.

695-699, doi: 10.1109/ISRITI56927.2022.10052867.

[22] L. Handayani, A. Abu-Siada, S. Suwarno, N. Hariyanto, and M. R. Djalal, "Power System Performance Enhancement using Superconducting Magnetic Energy Storage unit and Proportional Integral Derivative Control," in *2020 2nd International Conference on Smart Power & Internet Energy Systems (SPIES)*, 15-18 Sept. 2020 2020, pp. 281-286, doi: 10.1109/SPIES48661.2020.9242922.

[23] R. S. Utami, A. Abu-Siada, Suwarno, N. Hariyanto, M. R. Djalal, and J. Hartono, "Optimal Tuning of Unified Power Flow Controller Using Firefly Algorithm to Improve Damping of Inter-Area Oscillations in Multi-Machine System," in *2020 2nd International Conference on Smart Power & Internet Energy Systems (SPIES)*, 15-18 Sept. 2020 2020, pp. 436-441, doi: 10.1109/SPIES48661.2020.9243095.

[24] W. Aribowo, "Tuning For Power System Stabilizer Using Distributed Time-Delay Neural Network," *SINERGI,* vol. 22, no. 3, pp. 205-210, 2018, doi: 10.22441/sinergi.2018.3.009.

[25] N. Kadir and M. R. Djalal, "Optimal Design Pss-Pid Control On Single Machine Infinite Bus Using Ant Colony Optimization," *SINERGI,* vol. 25, no. 2, pp. 169-176, 2021, doi: 10.22441/sinergi.2021.2.008.

[26] I. Manuaba, M. Abdillah, R. Zamora, and H. Setiadi, "Adaptive Power System Stabilizer Using Kernel Extreme Learning Machine," *International Journal of Intelligent Engineering & Systems,* vol. 14, no. 3, 2021, doi: 10.22266/ijies2021.0630.39.

[27] M. Y. Yunus, M. R. Djalal, and M. Marhatang, "Optimal Design Power System Stabilizer Using Firefly Algorithm in Interconnected 150 kV Sulselrabar System, Indonesia," *Internatioanl Review of Electrical Engineering (IREE)*, vol. 12, no. 3, pp. 250-259, 2017, doi: 10.15866/iree.v12i3.11136.

[28] I. Robandi, "Modern Power System Control," *Penerbit ANDI, Yogyakarta,* 2009.

[29] K. R. Padiyar, *Power System Dynamics.* John Wiley & sons Ltd, Interlaine Publishing Ltd, 1996.

[30] S. Suharto, I. Robandi, and A. Priyadi, "Power System Stabilizer (PSS) Tuning for Dynamic Stability Improvement in Power Systems Using Bat Algorithm (BA)," *Jurnal Teknik ITS,* vol. 4, no. 1, pp. B4-B9, 2015, doi: 10.12962/j23373539.v4i1.8613.

[31] A. Khan, H. Hizam, N. I. Abdul-Wahab, and M. L. Othman, "Solution of optimal power flow using non-dominated sorting multi objective based hybrid firefly and particle swarm optimization algorithm," *Energies,* vol. 13, no. 16, p. 4265, 2020, doi: 10.3390/en13164265.